Solar Energy Materials & Solar Cells 282 (2025) 113403

Contents lists available at ScienceDirect

Solar Energy Materials and Solar Cells

journal homepage: www.elsevier.com/locate/solmat

Low-temperature ZnO_x (ALD)/SiO_2 (spin-coating) dopant-free electron-selective contact enabling 22.11%-efficiency Si solar cell

Jiawang Qiu [a], Ying Zhang [a], Zhongguo Zhou [a], Xi Lin [a], Xiaomin Song [a], Sihua Zhong [a], Haipeng Yin [b], Xiulin Jiang [b], Junbing Zhang [b], Zi Ouyang [b], Wenzhong Shen [c], Zengguang Huang [a,*]

[a] School of Science, Jiangsu Ocean University, 222005, Lianyungang, Jiangsu Province, PR China
[b] JA Solar, 225131, Yangzhou, Jiangsu Province, PR China
[c] School of Physics and Astronomy, and Institute of Solar Energy, Shanghai Jiao Tong University, 200240, Shanghai, PR China

ARTICLE INFO

Keywords:
Dopant-free
Electron-selective
Passivating contacts
ALD-ZnO_x
Spin-coating SiO_2

ABSTRACT

In recent years, there has been a concerted effort to develop new electron-selective (ES) materials for crystalline silicon (c-Si) solar cells aimed at simplifying the processes and improving efficiencies. By combing the low-temperature spin-coating SiO_2 with the atomic layer deposition (ALD) ZnO_x, we in this work prepared the dopant-free ES contact of ALD-ZnO_x/Spin-coating SiO_2/LiF/Al and applied it to n-type c-Si solar cells as a full-area rear contact. It is found that the optimal ZnO_x/SiO_2/LiF/Al sample with the 10 cycles-thickness ZnO_x, has the lowest contact resistivity (ρ_c) of 0.857 mΩ cm^2 and the high minority carrier lifetime (τ_{eff}) of 319.43 μs, indicating the simultaneous achievement of the excellent contact performance and surface passivation. It is verified that the spin-coating SiO_2 layer can boost the surface passivation level while maintaining the low ρ_c due to the pinhole-like carrier transport mechanism in spin-coating SiO_2. Finally, the champion efficiency of 22.11 % was achieved in the n-type c-Si solar cell with full-area rear ZnO_x/SiO_2/LiF/Al ES dopant-free contact. This represents the best performance for ZnO_x-based dopant-free c-Si solar cells, displaying a bright prospect of this ES contact in the low-temperature and high-efficiency Si heterojunction and Si/Perovskite tandem solar cells.

1. Introduction

Carrier-selective contact (CSC) is widely used in crystalline silicon (c-Si) solar cells due to its high efficiency and simple process [1–8]. As this technology continues to evolve, the requirements for hole-selective (HS) layers and electron-selective (ES) layers are becoming increasingly demanding [9–12]. The ES layers as the electron transport channel should simultaneously possess superior interface passivation and low resistivity. Therefore, the development of suitable ES layers materials to meet electrical requirements is crucial for further improving the performance of Si-based solar cells.

Transition metal oxide (TMO) layers are widely applied in c-Si solar cells due to their excellent band alignment properties and work functions [13–15]. These dopant-free, wide-bandgap, simple-process, and low-cost TMOs have their own superiorities compared to the traditional CSCs of the doped silicon suffering from parasitic absorption and Auger recombination losses [16–18]. Zinc oxide (ZnO) as a high-electron-mobility, wide-bandgap, non-toxicity, and low-cost TMO based ES layers materials [19–21], is extensively used in polymer solar cells, dye-sensitized solar cells, and perovskite solar cells [22–25]. Zhang et al. developed a highly conductive boron-doped ZnO (BZO) using metal-organic chemical vapor deposition (MOCVD) and fabricated a structure of a-Si: H/BZO in 2017, obtaining a power conversion efficiency (PCE) of only 16.6 % [26]. In 2018, Ding et al. prepared a-Si: H/ZnO: Al as an ES layers by employing spin-coating technique, and achieved a PCE of 18.46 % [27]. Next year, Zhong et al. successfully achieved a PCE of 19.5 % using a-Si: H/AZO (magnetron sputtering)/Al as an ES contact [28]. Later, in 2019, they fabricated a solar cell with a-Si: H/ZnO_x/LiF contact, demonstrating a contact resistivity (ρ_c) of 136 mΩ cm^2 and a higher PCE of 21.4 % [29].

Despite the reported superiorities of the ZnO thin film in the published work, achieving simultaneous excellent passivation and electrical conductivity remains a challenge, thereby limiting the improvement of device PCE. Beh et al.'s work indicates that ALD-ZnO exhibits very low

* Corresponding author.
E-mail address: zghuang@jou.edu.cn (Z. Huang).

https://doi.org/10.1016/j.solmat.2025.113403
Received 9 November 2024; Received in revised form 18 December 2024; Accepted 2 January 2025
Available online 8 January 2025

ρ_cs, highlighting its exceptional electron transport capacity compared to sputtering-deposited ZnO [30]. To achieve an excellent surface passivation under conditions of low ρ_c, we in our previous work prepared the spin-coating SiO_2 layer on the ALD-AlO_x passivated c-Si wafer, and found that the spin-coating SiO_2 layer was able to greatly improve the surface passivation while keeping the ultralow ρ_c. The key factor for the simultaneous achievement of the excellent passivation and ultralow ρ_c lies to the pinhole-like carrier transport mechanism in the spin-coating SiO_2 layer [31]. The successful application of the spin-coating SiO_2 paves a broad way for its further use in the high-performance dopant--free c-Si solar cell.

In this work, we have developed ALD-ZnO_x/spin-coating SiO_2/LiF/Al as an ES contact for the rear surface of n-type Si solar cells. This novel design effectively addresses the previously mentioned issues of achieving both excellent surface passivation and ultralow ρ_c simultaneously. Thanks to the pinhole-like carrier transport mechanism in the spin-coating SiO_2 layer, the c-Si/ZnO_x/SiO_2/LiF/Al ES contact exhibits a remarkably low ρ_c of 0.857 mΩ cm^2 and a 36.3 % increase in the τ_{eff}. Finally, we achieved a champion efficiency of 22.11 %, surpassing those of the reported ZnO-based solar cells. Our findings underscore the significant potential of ZnO_x/SiO_2/LiF/Al as an ES contact layer for c-Si solar cells, further validating the promising application prospects of spin-coating SiO_2 on solar cells.

2. Results and discussion

As shown in Fig. 1, utilizing high-angle-annular-dark-field scanning transmission electron microscopy (HAADF–STEM), we obtained the interfacial structure and elemental distribution of the rear c-Si/ZnO_x/SiO_2/LiF/Al. The high-resolution cross-sectional STEM image Fig. 1a and the magnified image Fig. 1b clearly display that the rear structure is made up of a continuous SiO_2 layer (~10 nm), a ZnO_x layer (~1 nm), a LiF layer (~1.2 nm), and an Al layer.

This distinguished structure can be confirmed by the EDS (Energy Dispersive Spectroscopy) elemental mappings of Si, O, F, and Al elements as shown in Fig. 1c. It is worth noting that the EDS elemental

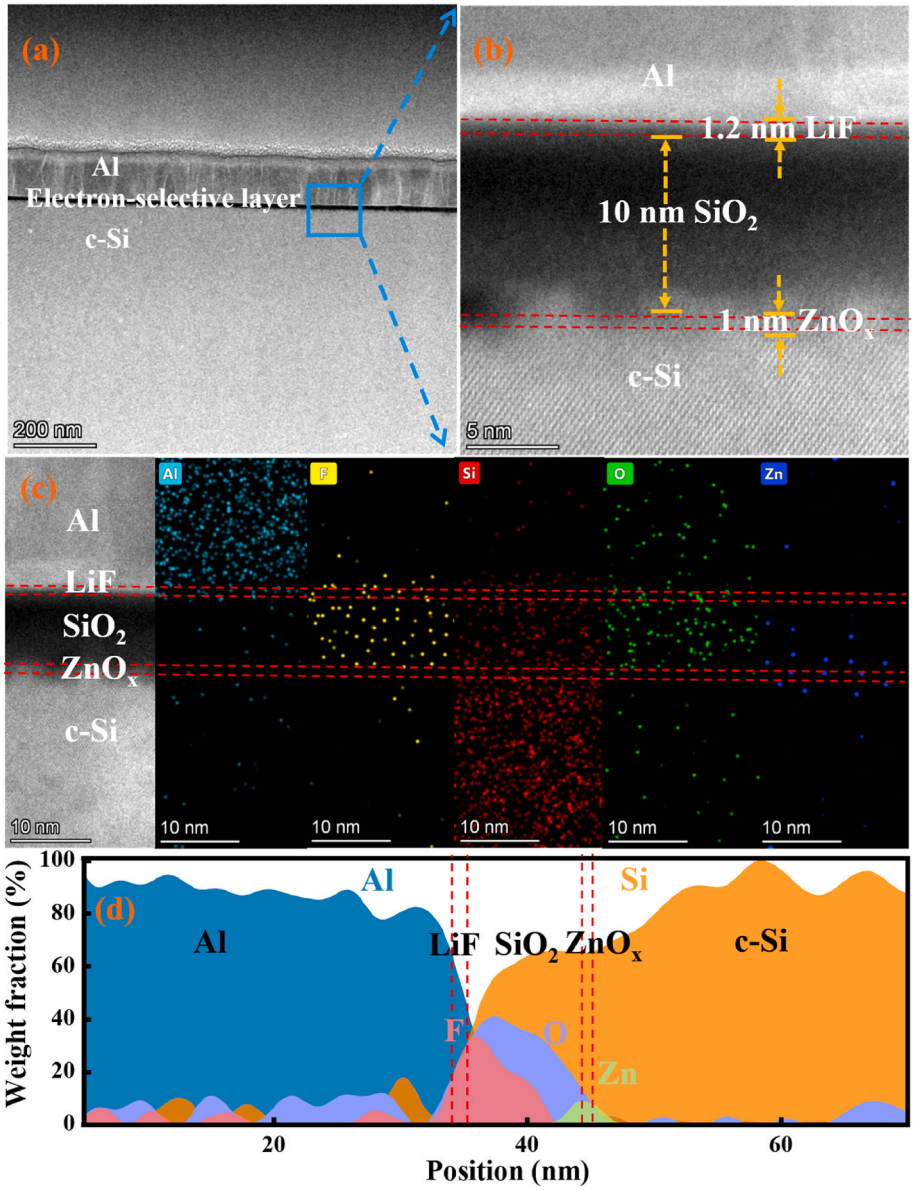

Fig. 1. a) HAADF-STEM microscopy images of the c-Si/ZnO_x/SiO_2/LiF/Al. b) High-resolution microscopy image of c-Si/ZnO_x/SiO_2/LiF/Al contact. c) HAADF–STEM and EDS element mappings of Si, O, F, Zn, and Al at the c-Si/ZnO_x/SiO_2/LiF/Al interface. d) Energy-dispersive X-ray spectroscopy line scan of a c-Si/ZnO_x/SiO_2/LiF/Al interface.

mappings show the diffusion of Al and F elements into the SiO_2 layer, which is demonstrated more clearly by the Energy-dispersive X-ray spectroscopy line scan of Fig. 1d. The diffusion behavior of Al and F elements is mainly attributed to the loose and porous structures of SiO_2 layer during the spin-coating process, which is consistent with the result of the previous work [31].

Fig. 2 shows the XPS measurements of the ALD-ZnO_x and spin-coating SiO_2 films. The O 1*s* spectrum of the spin-coating SiO_2 is shown in Fig. 2a, which can be divided into two peaks with binding energies of 532.66 eV and 532.94 eV, respectively. Both of these binding energy peaks correspond to the Si-O bond [32–34].

Fig. 2b shows the Si 2*p* peak of the spin-coating SiO_2, which can be divided into two peaks with binding energies of 103.37 eV and 103.64 eV. These peaks correspond to Si 2*p*3/2 and Si 2*p*1/2, respectively [32,33]. No peak for the Si element is observed at 99.3 eV, indicating that it exists only in the oxidized state [35,36]. As shown in Fig. 2c, the O 1s spectrum of ALD-ZnO_x, based on Gaussian fitting, can be divided into two peaks with binding energies of 530.66 eV and 531.51 eV, respectively. The 530.66 eV peak indicates Zn-O bonds [37]. The higher binding energy peak (531.51 eV) is mainly due to the adsorption of specific products on the surface of ALD-ZnO_x films, such as -CO_3, H_2O, and other corresponding hydroxides [38,39]. Fig. 2d further shows the Gaussian fitting of Zn 2*p* peaks. The 1021.62 eV and 1044.15 eV peaks correspond to Zn 2*p*3/2 and Zn 2*p*1/2, respectively. The binding energy for metallic zinc at 1021.5 eV is not observed, which suggests the absence of interstitial zinc [40]. Thus, it can be concluded that the Zn element in our ALD-grown film exists only in the oxidized state.

Excellent passivation contact performance demands both a low recombination current density (J_0) and a low ρ_c, as described by Eq. (1) [41].

$$S_{10} = log_{10}\left(\frac{V_{th}/J_0}{\rho_c}\right) \quad (1)$$

Consequently, we in this section focus on the τ_{eff} which is related to J_0, and the ρ_c. Fig. 3a shows the differences of ρ_cs before and after spin-coating SiO_2 for the samples with 5, 10, 20, 30, and 40 cycles ZnO_x. Note that the growth per cycle (GPC) of ZnO_x is ~0.1 nm. By using the transfer length method (TLM), we extracted the ρ_c values of the c-Si/ZnO_x/LiF/Al and c-Si/ZnO_x/SiO_2/LiF/Al structures from the current-voltage (*I-V*) measurements. Although we observed an increase trend of ρ_c as the increasing thickness of the ZnO_x for the samples with only ZnO_x thin film, all the ρ_c values were kept in the range of 0.458–5.83 mΩ cm^2. After spin-coating SiO_2, all the corresponding ρ_c values showed slightly increases, but these values are still kept below 7 mΩ cm^2. Obviously, the c-Si/ZnO_x/LiF/Al and c-Si/ZnO_x/SiO_2/LiF/Al samples corresponding 10-cycle ZnO_x have the lowest ρ_c values of 0.458 mΩ cm^2 and 0.857 mΩ cm^2, respectively (see Fig. S1). The low ρ_cs of the before and after spin-coating SiO_2 reveals that the influence of the thick spin-coating SiO_2 on the ρ_c can be neglected, which is beneficial to obtaining high *FF* of the devices. According to previous work [31], the pinhole-like carrier transport the spin-coating SiO_2 layer determines the characteristic of low resistivity that is independent of thickness.

Next, we examine the comparison of surface passivation before and after spin-coating SiO_2 on the samples with different ZnO_x thicknesses as shown in Fig. 3b. The samples with only ZnO_x thin film show the increasing τ_{eff}s with the increase of ZnO_x thicknesses. Importantly, after spin-coating SiO_2, the τ_{eff}s of all samples demonstrate significantly improvements. For example, the τ_{eff}s of the sample with the stack of 40-cycle ZnO_x and spin-coating SiO_2 reach up to 358.97 μs with a relative increase of 34.4 % comparing with the 267.19 μs of the sample with only 40-cycle ZnO_x. The relative increase of the τ_{eff} is even up to 36.3 % in the case of 10-cycle ZnO_x, corresponding to the τ_{eff}s value of 234.33 μs (before spin-coating SiO_2) and the τ_{eff}s value of 319.43 μs (after spin-coating SiO_2) as shown in Fig. 3c. This significant enhancement can be attributed to the substantial improvement in the chemical passivation effect, where the oxygen atoms in the SiO_2 layer effectively bond with the dangling bonds in the silicon substrate, forming a stable Si-O chemical bond [31,42].

Fig. 4a illustrates the n-type solar cell with the full-area ZnO_x/SiO_2/LiF/Al ES contact. Utilizing 170 μm-thickness, n-type [100] Cz c-Si wafers of 1–3 Ω cm resistivity, the cell's front incorporates p^+ emitters, Al_2O_3/SiN_x (PECVD), and Ag (screen-printed), while the back is featured ZnO_x (10-cycle, ALD), SiO_2 (~10 nm, spin-coating), and LiF/Al (1.2 nm/200 nm, thermal evaporation). The reference solar cell has the similar structure and the same processes with the above solar cell, except that it lacks a spin-coating SiO_2 layer.

Fig. 4b demonstrates the current density-voltage (*J-V*) curves and detailed output parameters for an n-type solar cell featuring a full-area ZnO_x/SiO_2/LiF/Al ES contact under AM 1.5 G standard illumination, in comparison to those of the reference solar cell with no spin-coating SiO_2. Notably, the highest efficiency of 22.11 % was achieved on the solar cell with spin-coating SiO_2, along with a high short-circuit current

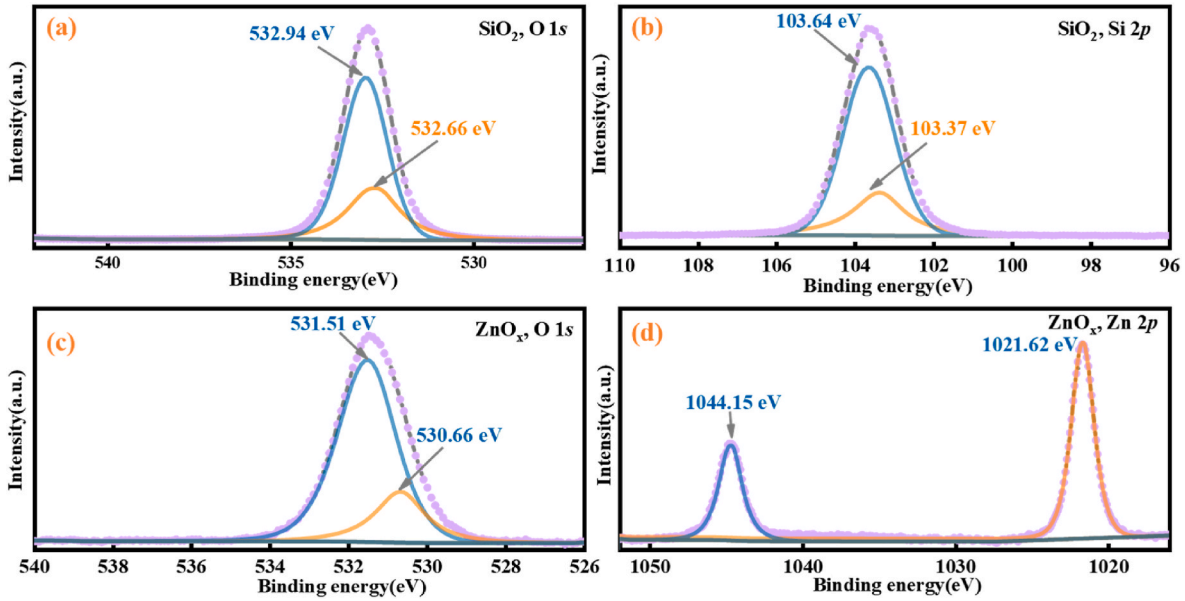

Fig. 2. XPS spectra of spin-coating SiO_2 and ALD-ZnO_x films: a) O 1*s*, b) Si 2*p* for spin-coating SiO_2; c) O 1*s*, d) Zn 2*p* for ALD-ZnO_x.

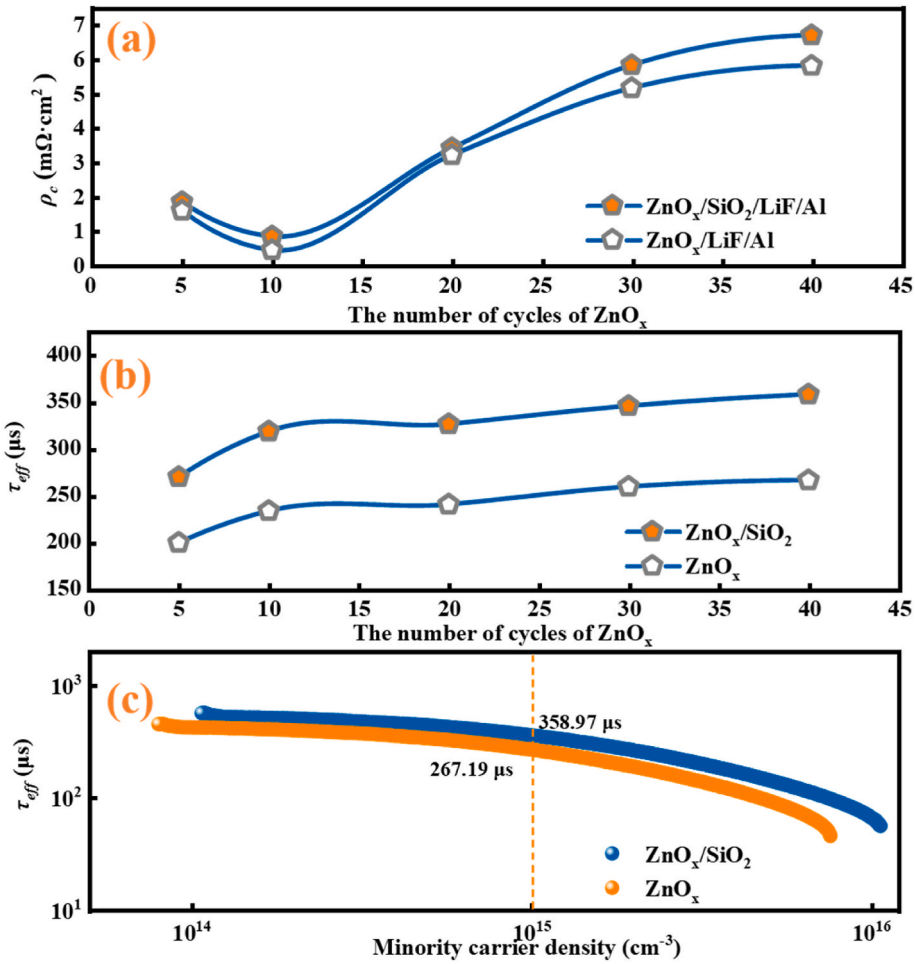

Fig. 3. a) The ρ_cs of the samples with different ZnO_x thicknesses in the case of before and after spin-coating with SiO_2. b) The τ_{eff}s of the samples with different ZnO_x thicknesses in the case of before and after spin-coating with SiO_2. c) The comparison of *τ_{eff} curves for the before and after spin-coating SiO_2 sample in the case of 40-cycle* ZnO_x.

density (J_{sc}) of 40.44 mA cm^{-2}, an open circuit voltage (V_{oc}) of 663.40 mV, and a high fill factor (*FF*) of 82.42 %. In contrast, the ZnO_x/LiF/Al contact solar cell with no spin-coating SiO_2 only has an efficiency of 19.25 %, with a J_{sc} of 38.27 mA cm^{-2}, a V_{oc} of 607.23 mV, and an *FF* of 82.84 %. This comparison highlights an absolute efficiency improvement of 2.86 % for the optimal device. The device's enhanced performance origins from a 5.67 % and 9.25 % increase in J_{sc} and V_{oc}, from 38.27 mA cm^{-2} to 40.44 mA cm^{-2} and from 607.23 mV to 663.40 mV, respectively, while there is a slight decrease in the *FF* from 82.84 % to 82.42 %. The improvement of J_{sc} and V_{oc} is attributed to the enhanced surface passivation from the spin-coating SiO_2 layer. As discussed in the above part, the spin-coating SiO_2 does not significantly affect the ρ_c, allowing the device to maintain a high *FF*.

To analyze the spectral response of the device, Fig. 4c further displays the external quantum efficiencies (EQEs) of the devices before and after the spin-coating SiO_2 layer. The cells both with and without the SiO_2 layer possess high EQEs in the short and medium wavelength range of 300–800 nm, due to the excellent passivation and antireflection properties of the Al_2O_3/SiN_x stacks on the front surface. Solar cells with the spin-coating SiO_2 layer on the back exhibit notably higher EQEs in the long wavelength range of 800 nm–1100 nm than the device without the SiO_2 layer. Moreover, the J_{sc} value of 40.44 mA cm^{-2} for the ZnO_x/SiO_2/LiF solar cell in Fig. 4b is consistent with the integral value of 40.67 mA cm^{-2} by the corresponding EQEs in Fig. 4c. In addition, Fig. 4d shows the reflectance (R) and internal quantum efficiencies (IQEs), revealing that the gain in EQEs is due to electrical rather than optical improvement. Obviously, this improvement in long wavelength spectral response is attributed to the presence of the spin-coating SiO_2 layer, which is consistent with the result of the *J-V* analysis.

3. Conclusions

In summary, an ES dopant-free passivating contact with low-temperature ALD-ZnO_x/Spin-coating SiO_2/LiF/Al was prepared on the rear side of n-type c-Si solar cell, and the interfacial structures were clearly shown by the HAADF–STEM, the EDS elemental mappings and the XPS spectra. Furthermore, the influence of the ZnO_x layer thickness on the ρ_c and surface passivation τ_{eff} was investigated, displaying that the structure with 10 nm-thickness ZnO_x possesses the lowest ρ_c of 0.857 mΩ cm^2 and the high τ_{eff} of 319.43 μs. The simultaneous achievement of the ultralow ρ_c and the high τ_{eff} is attributed to the pinhole-like carriers transfer mechanism in the spin-coating SiO_2 layer. Finally, we achieved the highest PCE of 22.11 % on the device with 10 nm-thickness ZnO_x, as well as the J_{sc} of 40.44 mA cm^{-2}, V_{oc} of 663.40 mV, and *FF* of 82.42 %. By combining with the low-temperature, simple-process and low-cost spin-coating SiO_2 layer, we achieved the record PCE of the ZnO_x-based dopant-free solar cell, revealing the great potential of this ES contact in high-efficiency c-Si and Si/Perovskite tandem solar cells.

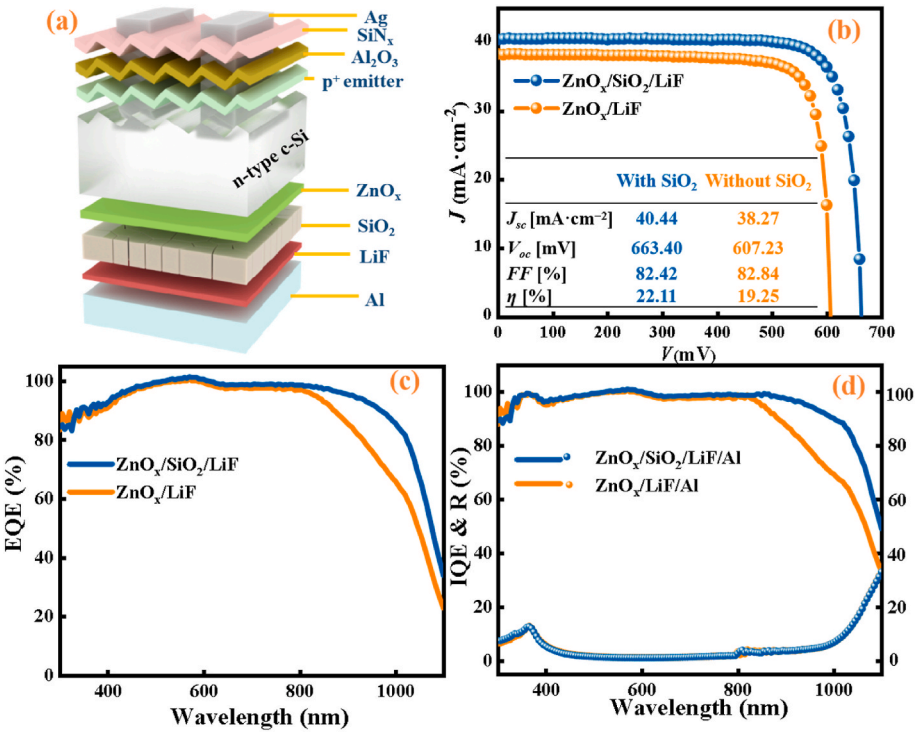

Fig. 4. a) Schematic diagram of n-type passivating contact solar cell with a rear full-area ZnO_x/SiO_2/LiF ES contact. b) *J-V* curves and output parameters of n-type passivating contact solar cells with ZnO_x/SiO_2/LiF/Al and ZnO_x/LiF/Al contact structures. c) EQEs curves of ZnO_x/SiO_2/LiF/Al and ZnO_x/LiF/Al contact structures. d) IQEs (top lines) and R (bottom lines) spectra for the devices with the ZnO_x/SiO_2/LiF/Al and ZnO_x/LiF/Al rear contacts.

4. Experimental section

Preparation of samples: n-type float zone (FZ) c-Si wafers with (100) orientation, a resistivity of 4–7 Ω cm, and a thickness of 450 ± 10 μm were used as substrates. The c-Si wafers were put into an acetone solution for ultrasonic cleaning for 30 min to clean the organic substances on the surface. Next, the wafers were cleaned by the Radio Corporation of America (RCA) cleans 1 & 2 [43], followed by being immersed in HF (1%–2%) solution to remove the SiO_x layer formed in the RCA cleaning process. To obtain the τ_{eff}s before and after spin-coating SiO_2, the cleaned wafers were coated with different thicknesses of ZnO_x on both sides using ALD, employing dimethylzinc as the zinc source and deionized (DI) water as the oxidant. Subsequently, the samples were positioned on the spin coater's pad for the spin-coating process. During this process, 30 μl of sol-gel solution was applied uniformly onto the wafer using a pipette gun at the rotational speed of 4000 rpm. The solution had a molar concentration of 0.06 mol/L, prepared from a tetraethyl orthosilicate precursor, isopropanol (IPA), DI water, and nitric acid. Finally, the samples were annealed at 100 °C for 3 min. The details of the solution preparation and the spin-coating process are given in our earlier publication [31]. To further explore the contact characteristics of spin-coating SiO_2, the ρ_cs of different ES contacts on solar-grade Cz silicon wafers were evaluated, including the stacks of ZnO_x/LiF/Al and ZnO_x/SiO_2/LiF/Al, where the LiF/Al stack was deposited via thermal evaporation. ZnO_x thin films were prepared using 5, 10, 20, 30, and 40 cycles of ALD.

Preparation of devices: The c-Si solar cells (2×2 cm^2) were fabricated on solar-grade Cz n-type wafers with a thickness of 170 μm. Fabrication of the front structure involved standard cleaning, saw-damage removal, thermal boron diffusion, and edge etching. Subsequently, an Al_2O_3 passivation layer and a SiN_x antireflection layer were deposited on the p^+ emitter using ALD and PECVD, respectively. Front Ag grids were prepared via screen printing silver paste. For the rear side, ZnO_x was prepared using ALD. The aged sol-gel solution was spin-coated to produce approximately 10 nm-thickness SiO_2, and the LiF/Al stack was formed via thermal evaporation. The conceptual diagram of ALD-ZnO_x steps, spin-coating SiO_2, and thermal evaporation LiF/Al on the back surface of the solar cell mentioned above is shown in Fig. 5.

Characterizations: The cross-sectional images of c-Si/ZnO_x/SiO_2/LiF/Al (170 μm/1 nm/10 nm/1.2 nm/200 nm) ES layers structure were obtained using the HAADF-STEM (Titan Themis G2 60–300, Thermo Fisher) coupled with energy-dispersive X-ray spectroscopy. The atomic composition and chemical states of the ZnO_x/SiO_2/LiF film were analyzed using XPS (K-Alpha, Thermo Fisher) with monochromatic Al Kα X-ray (photon energy of 1486.6 eV). The surface passivation measurements by a lifetime tester (Sinton Instruments, WCT-120) in quasi-steady state photoconductance (QSSPC). The contact resistivity was obtained using the TLM method. The electrode length in the TLM pattern was 2 mm and the pad spacing was 0.5, 1, 1.5, 2, 3, and 4 mm, respectively. The solar cells' *J-V* characteristics were investigated under the illumination of AM1.5G using a Newport 92250 A-1000 solar cell *I-V* tester and a Keithley 2400 source meter. The EQEs were measured by a Crowntech QTEST HIFINITY 5 system.

CRediT authorship contribution statement

Jiawang Qiu: Writing – original draft, Validation, Methodology, Investigation, Formal analysis, Data curation, Conceptualization. **Ying Zhang:** Investigation. **Zhongguo Zhou:** Investigation. **Xi Lin:** Conceptualization. **Xiaomin Song:** Conceptualization. **Sihua Zhong:** Conceptualization. **Haipeng Yin:** Resources. **Xiulin Jiang:** Conceptualization. **Junbing Zhang:** Conceptualization. **Zi Ouyang:** Methodology. **Wenzhong Shen:** Methodology. **Zengguang Huang:** Writing – review & editing, Visualization, Validation, Supervision, Resources, Project administration, Methodology, Funding acquisition, Conceptualization.

Declaration of competing interest

The authors declare that they have no known competing financial interests or personal relationships that could have appeared to influence

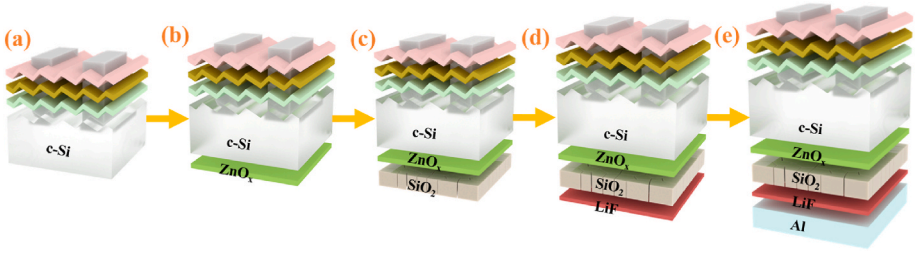

Fig. 5. Process flow of the rear structure of the solar cell. a) The front side as-prepared cell sample, b) ALD-ZnO_x, c) spin-coating SiO_2, d) thermal evaporation LiF and e) thermal evaporation Al.

the work reported in this paper.

Acknowledgments

This work was supported by the Natural Science Foundation of Jiangsu Province (BK20221395), the "Qinglan" Project of Jiangsu Education Department, the Natural Science Foundation of China (61774069, 62104086, 11834011, 11974242), the Postgraduate Research & Practice Innovation Program of Jiangsu Ocean University (KYCX2024-22) and Jiangsu Province (KYCX23_3459).

Appendix A. Supplementary data

Supplementary data to this article can be found online at https://doi.org/10.1016/j.solmat.2025.113403.

Data availability

Data will be made available on request.

References

[1] Z. Wang, J. He, W. Wang, H. Lin, Z. Xu, Q. Liu, S. Peng, J. Hou, D. He, P. Gao, Twenty percent efficiency crystalline silicon solar cells with solution-processed electron-selective contacts, ACS Appl. Energy Mater. 4 (2021) 3644–3650.
[2] A. Tyagi, J. Biswas, K. Ghosh, A. Kottantharayil, S. Lodha, Performance analysis of silicon carrier selective contact solar cells with ALD MoOx as hole selective layer, Silicon 14 (2022) 1663–1670.
[3]] J. Bullock, M. Hettick, J. Geissbühler, A.J. Ong, T. Allen, Carolin M. Sutter-Fella, T. Chen, H. Ota, E.W. Schaler, S. De Wolf, C. Ballif, A. Cuevas, A. Javey, Efficient silicon solar cells with dopant-free asymmetric heterocontacts, Nat. Energy 1 (2016) 15031.
[4] U. Würfel, A. Cuevas, P. Würfel, Charge carrier separation in solar cells, IEEE J. Photovoltaics 5 (2015) 461–469.
[5] G. Du, L. Li, X. Yang, X. Zhou, Z. Su, P. Cheng, Y. Lin, L. Lu, J. Wang, L. Yang, X. Gao, X. Chen, D. Li, Improved V2OX passivating contact for p-type crystalline silicon solar cells by oxygen vacancy modulation with a SiOX tunnel layer, Adv. Mater. Interfac. 8 (2021) 2100989.
[6] L. Lu, Y. Zeng, M. Liao, J. Zheng, Y. Lin, M. Feng, Y. Zhi, H. He, W. Ding, C. Shou, G. Qin, B. Yan, J. Ye, Dopant diffusion through ultrathin AlOx and AlOx/SiOx tunnel layer in TOPCon structure and its impact on the passivation quality on c-Si solar cells, Sol. Energy Mater. Sol. Cell. 223 (2021) 110970.
[7] X. Yang, P. Zheng, Q. Bi, K. Weber, Silicon heterojunction solar cells with electron selective TiOx contact, Sol. Energy Mater. Sol. Cell. 150 (2016) 32–38.
[8] Y. Liu, L. Zhang, H. Cheng, X. Song, S. Zhong, L. Shi, Z. Huang, Electron-Selective contacts ATO/LiF/Al-based high-performance N-type silicon solar cells, Adv. Mater. Interfac. 9 (2022) 2201512.
[9] Z. Wang, Y. Yang, L. Zhang, H. Lin, Z. Zhang, D. Wang, S. Peng, D. He, J. Ye, P. Gao, Modulation-doped ZnO as high performance electron-selective layer for efficient silicon heterojunction solar cells, Nano Energy 54 (2018) 99–105.
[10] Z. Huang, S. Zhong, X. Hua, X. Lin, X. Kong, N. Dai, W. Shen, An effective way to simultaneous realization of excellent optical and electrical performance in large-scale Si nano/microstructures, Prog. Photovoltaics Res. Appl. 23 (2015) 964–972.
[11] H. Cheng, Z. Huang, L. Zhang, Y. Liu, X. Song, R. Tong, S. Zhong, L. Shi, X. Kong, W. Shen, 21.16%-efficiency p-type TOPCon solar cell with ALD-Al2O3/MoOx/Ag as a hole-selective passivating contact, Sol. Energy 247 (2022) 171–176.
[12] J. Li, Q. Kang, Y. Wang, Z. Zhou, Z. Sun, H. Zhang, W. Lu, X. Tao, S.T. Zhang, X. Chen, Z. Zheng, H. Yan, D. Li, Y. Zhang, Low oxygen content MoOx and SiOx tunnel layer based heterocontacts for efficient and stable crystalline silicon solar cells approaching 22% efficiency, Adv. Funct. Mater. 34 (2023) 2310619.
[13] S. Cao, J. Li, Y. Lin, T. Pan, G. Du, J. Zhang, L. Yang, X. Chen, L. Lu, N. Min, M. Yin, D. Li, Interfacial behavior and stability analysis of p-type crystalline silicon solar cells based on hole-selective MoO/metal contacts, Sol. RRL 3 (2019) 1900274.
[14] M.M. Makhlouf, M.M. Shehata, Multilayer emitter of molybdenum oxide/silver/molybdenum oxide thin films for silicon heterojunction solar cells: device fabrication and electrical characterization, J. Alloys Compd. 904 (2022) 164102.
[15] Y. Liu, B. Sang, M.A. Hossain, K. Gao, H. Cheng, X. Song, S. Zhong, L. Shi, W. Shen, B. Hoex, Z. Huang, A novel passivating electron contact for high-performance silicon solar cells by ALD Al-doped TiO2, Sol. Energy 228 (2021) 531–539.
[16] Y. Wan, S.K. Karuturi, C. Samundsett, J. Bullock, M. Hettick, D. Yan, J. Peng, P. R. Narangari, S. Mokkapati, H.H. Tan, C. Jagadish, A. Javey, A. Cuevas, Tantalum oxide electron-selective heterocontacts for silicon photovoltaics and photoelectrochemical water reduction, ACS Energy Lett. 3 (2018) 125–131.
[17] L. Zhang, J. Qiu, H. Cheng, Y. Zhang, S. Zhong, L. Shi, H. Yin, R. Tong, Z. Sun, W. Shen, X. Song, Z. Huang, Low-temperature Ta-doped TiOx electron-selective contacts for high-performance silicon solar cells, Sol. Energy Mater. Sol. Cell. 266 (2024) 112703.
[18] Z.G. Huang, K. Gao, X.G. Wang, C. Xu, X.M. Song, L.X. Shi, Y. Zhang, B. Hoex, W. Z. Shen, Large-area MACE Si nano-inverted-pyramids for PERC solar cell application, Sol. Energy 188 (2019) 300–304.
[19] K. Ellmer, A. Klein, B. Rech, Transparent Conductive Zinc Oxide : Basics and Applications in Thin Film Solar Cells, Springer, 2008, p. 104.
[20] J. Perrenoud, L. Kranz, S. Buecheler, F. Pianezzi, A.N. Tiwari, The use of aluminium doped ZnO as transparent conductive oxide for CdS/CdTe solar cells, Thin Solid Films 519 (2011) 7444–7448.
[21] M. Morales-Masis, S. De Wolf, R. Woods-Robinson, J.W. Ager, C. Ballif, Transparent electrodes for efficient optoelectronics, Advanced Electronic Materials 3 (2017) 1600529.
[22] S. Chen, J.R. Manders, S.-W. Tsang, F. So, Metal oxides for interface engineering in polymer solar cells, J. Mater. Chem. 22 (2012) 24202–24212.
[23] J. You, C.C. Chen, L. Dou, S. Murase, H.S. Duan, S.A. Hawks, T. Xu, H.J. Son, L. Yu, G. Li, Y. Yang, Metal oxide nanoparticles as an electron-transport layer in high-performance and stable inverted polymer solar cells, Adv. Mat. (Deerfield Beach, Fla.) 24 (2012) 5267–5272.
[24] J. Tian, Q. Zhang, E. Uchaker, R. Gao, X. Qu, S. Zhang, G. Cao, Architectured ZnO photoelectrode for high efficiency quantum dot sensitized solar cells, Energy Environ. Sci. 6 (2013) 3542–3547.
[25] C. Fei, J. Tian, Y. Wang, X. Liu, L. Lv, Z. Zhao, G. Cao, Improved charge generation and collection in dye-sensitized solar cells with modified photoanode surface, Nano Energy 10 (2014) 353–362.
[26] F. Wang, S. Zhao, B. Liu, Y. Li, Q. Ren, R. Du, N. Wang, C. Wei, X. Chen, G. Wang, B. Yan, Y. Zhao, X. Zhang, Silicon solar cells with bifacial metal oxides carrier selective layers, Nano Energy 39 (2017) 437–443.
[27] J. Ding, Y. Zhou, G. Dong, M. Liu, D. Yu, F. Liu, Solution-processed ZnO as the efficient passivation and electron selective layer of silicon solar cells, Prog. Photovoltaics Res. Appl. 26 (2018) 974–980.
[28] S. Zhong, M. Morales-Masis, M. Mews, L. Korte, Q. Jeangros, W. Wu, M. Boccard, C. Ballif, Exploring co-sputtering of ZnO:Al and SiO2 for efficient electron-selective contacts on silicon solar cells, Sol. Energy Mater. Sol. Cell. 194 (2019) 67–73.
[29] S. Zhong, J. Dreon, Q. Jeangros, E. Aydin, S. De Wolf, F. Fu, M. Boccard, C. Ballif, Mitigating plasmonic absorption losses at rear electrodes in high-efficiency silicon solar cells using dopant-free contact stacks, Adv. Funct. Mater. 30 (2020) 1907840.
[30] H. Beh, D. Hiller, M. Zacharias, Optimization of ALD-ZnO thin films toward higher conductivity, Phys. Status Solidi 215 (2018) 1700880.
[31] J. Qiu, Z. Zhou, L. Zhang, X. Song, S. Zhong, H. Yin, R. Tong, J. Zhang, W. Shen, Z. Huang, Pinhole-like carriers transport in spin-coating SiO2 enabling high-efficiency dopant-free Si solar cells, Chem. Eng. J. (2024) 153672.
[32] J. He, Z. Ling, P. Gao, J. Ye, TiO2 films from the low-temperature oxidation of Ti as passivating-contact layers for Si heterojunction solar cells, Sol. RRL 1 (2017) 1700154.
[33] S.L. Pain, E. Khorani, T. Niewelt, A. Wratten, G.J. Paez Fajardo, B.P. Winfield, R. S. Bonilla, M. Walker, L.F.J. Piper, N.E. Grant, J.D. Murphy, Electronic characteristics of ultra-thin passivation layers for silicon photovoltaics, Adv. Mater. Interfac. 9 (2022) 2201339.
[34] R.A. Shircliff, P. Stradins, H. Moutinho, J. Fennell, M.L. Ghirardi, S.W. Cowley, H. M. Branz, I.T. Martin, Angle-resolved XPS analysis and characterization of monolayer and multilayer silane films for DNA coupling to silica, Langmuir 29 (2013) 4057–4067.

[35] T. Hattori, T. Nishina, Studies of SiO2 and Si-SiO2 interfaces by XPS, Surf. Sci. 86 (1979) 555–561.
[36] B. Ulgut, S. Suzer, XPS studies of SiO2/Si system under external bias, J. Phys. Chem. B 107 (2003) 2939–2943.
[37] L. Li, L. Fang, X.J. Zhou, Z.Y. Liu, L. Zhao, S. Jiang, X-ray photoelectron spectroscopy study and thermoelectric properties of Al-doped ZnO thin films, J. Electron. Spectrosc. Relat. Phenom. 173 (2009) 7–11.
[38] S.H. Jeong, J.H. Boo, Influence of target-to-substrate distance on the properties of AZO films grown by RF magnetron sputtering, Thin Solid Films 447–448 (2004) 105–110.
[39] W. Eisele, A. Ennaoui, P. Schubert-Bischoff, M. Giersig, C. Pettenkofer, J. Krauser, M. Lux-Steiner, S. Zweigart, F. Karg, XPS, TEM and NRA investigations of Zn(Se, OH)/Zn(OH)2 films on Cu(In,Ga)(S,Se)2 substrates for highly efficient solar cells, Sol. Energy Mater. Sol. Cell. 75 (2003) 17–26.
[40] M.N. Islam, T.B. Ghosh, K.L. Chopra, H.N. Acharya, XPS and X-ray diffraction studies of aluminum-doped zinc oxide transparent conducting films, Thin Solid Films 280 (1996) 20–25.
[41] J. Schmidt, R. Peibst, R. Brendel, Surface passivation of crystalline silicon solar cells: present and future, Sol. Energy Mater. Sol. Cell. 187 (2018) 39–54.
[42] S. Oh, S. Lee, E. Oh, S. Lim, Reduction of •Si≡Si3 defect density at the Si/SiO2 interface by sol-gel SiO2 thin film passivation, Thin Solid Films 632 (2017) 134–140.
[43] W. Kern, Cleaning solution based on hydrogen peroxide for use in silicon semiconductor technology, RCA Rev. 31 (1970) 187–206.